Structural correlation in water probed by hyper-Rayleigh scattering

David P. Shelton[a)]
Department of Physics and Astronomy, University of Nevada, Las Vegas, Nevada 89154-4002, USA

(Received 23 June 2017; accepted 3 October 2017; published online 17 October 2017)

Second-harmonic or hyper-Rayleigh scattering (HRS) is sensitive to molecular interactions and correlations, and there is a large coherent HRS contribution for water. This work shows that the distinctive angle and polarization dependence observed for HRS from water is due to the long-range orientation correlation of the molecules. The results of HRS experiments for water are analyzed in combination with a molecular dynamics simulation to determine the molecular hyperpolarizability and the short-range and long-range orientation correlation functions for the molecules. At long range, the longitudinal and transverse dipole-dipole orientation correlation functions are $B_L(r) = -2B_T(r) = a^3/r^3$ with $a = 0.166$ nm. Molecular correlation at distances $r > 100$ nm must be included to account for the HRS observations. *Published by AIP Publishing.* https://doi.org/10.1063/1.4991893

I. INTRODUCTION

Second-harmonic or hyper-Rayleigh scattering (HRS) is a nonlinear light scattering technique widely used to measure the first hyperpolarizability β of molecules in solution.[1,2] It is usually assumed that only incoherent scattering from the individual molecules contributes, and this is a good approximation for the contribution of a strong nonlinear optical chromophore in dilute solution, but it is not a good approximation for the solvent itself. Theoretical expressions including the coherent HRS contribution have been known from the earliest work,[3,4] but these expressions are not often applied to calculate the coherent HRS contribution since the correlations are usually unknown and changes in β due to the intermolecular interactions also significantly affect the HRS intensity. In simple liquids, the range of molecular correlation is assumed to be at most a few nm. In this case, correlations can affect the HRS intensity, but the angle and polarization dependence of HRS will be the same as for fully incoherent HRS from individual randomly oriented molecules.

The assumption that there are only short-range correlations in liquids is contradicted by the observed angle and polarization dependence of HRS for a number of polar liquids.[5–7] These HRS observations appear to require molecular orientation correlations on the scale of the optical wavelength, and the observed HRS angle and polarization dependence is found to match the functional form calculated for HRS from nonlocal polar modes of an isotropic liquid.[8] However, the origin and nature of such nonlocal polar modes was unclear, and a number of unsuccessful ideas were proposed and investigated. Most recently, the relations between HRS and correlation functions of a vector field have been investigated,[9,10] and it is now proposed that the dipole correlations known to exist in polar liquids account for the nonlocal polar modes and the HRS observations.

In the following work, the HRS observations for water are analyzed in combination with molecular dynamics (MD) simulation results, including the contributions of both the short-range correlations and long-range dipole correlations. The simplest model is assumed, with rigid molecules and a fixed average β tensor, to focus on the effect of orientation correlation without added complications. First the MD simulation results are presented, and then the HRS observations are presented and analyzed. The results presented below are in contrast to those in another recent work, which evaluated the HRS signal directly from a MD simulation trajectory and concluded that just short-range correlations can account for the HRS observations.[11] A similar analysis using the present MD simulation results is performed and compared with that work to reconcile the opposite conclusions. Then the analysis is extended to extract information about the molecular hyperpolarizability tensor β and the long-range orientation correlations in water. Long-range dipole correlations are found to be essential to account for the HRS observations.

II. MOLECULAR DYNAMICS SIMULATION

Molecular dynamics simulations were performed with the GROMACS software package (version 5.0.6)[12] using the rigid TIP4P/2005 water model.[13,14] Liquid water was simulated with 60 000 molecules in a 12.17 nm cubic box with periodic boundary conditions (PBC); long-range Coulomb interactions were treated by the particle mesh Ewald (PME) method with conducting boundary conditions, while Lennard-Jones (LJ) 6-12 interactions were treated using a 1.0 nm cutoff radius and analytical dispersion correction.[15] Temperature and pressure were controlled using a modified velocity rescaling thermostat and Berendsen barostat.[16] Equilibrium density at $T = 298$ K and $p = 101$ kPa was obtained using NPT simulation, while NVT simulation at the equilibrium density was used to determine the correlation functions. The NVT simulation was equilibrated for 1 ns before a 25 ns production run with 2 fs time steps.

[a)]shelton@physics.unlv.edu

TABLE I. MD simulation results for TIP4P/2005 water at $T = 298$ K.

Property	MD value
ρ (kg/m^3)	996
ρ (nm^{-3})	33.30
μ (D)	2.306
G_K	3.196
y[a]	6.011
g_K[b]	2.177
ε[c]	59.4
a^3 (10^{-3} nm^3)[d]	5.072
a (nm)	0.1718

[a]Equation (4).
[b]Equation (5).
[c]Equation (6).
[d]Equation (7).

Table I summarizes the results and Fig. 1 shows the correlation functions obtained from the MD simulation. Figure 1(a) shows the radial pair distribution function $g(r)$, Fig. 1(b) shows the orientation pair correlation function $F(r) = \langle \hat{\mu}_i \cdot \hat{\mu}_j \rangle = \langle \cos \theta_{ij}(r) \rangle$, while Fig. 1(c) shows the longitudinal and transverse dipole correlation functions $L(r) = \langle (\hat{\mu}_i \cdot \hat{r}_{ij})(\hat{\mu}_j \cdot \hat{r}_{ij}) \rangle$ and $T(r) = \frac{1}{2}[F(r) - L(r)]$ which enter the analysis of the HRS observations. The full, longitudinal, and transverse dipole-dipole correlation functions were calculated from the MD trajectory using the expressions[17]

$$F(r) = \left\langle \frac{1}{N} \sum_i \frac{1}{n_i(r)} \sum_{j=1}^{n_i(r)} (\hat{\mu}_i \cdot \hat{\mu}_j) \right\rangle, \tag{1}$$

$$L(r) = \left\langle \frac{1}{N} \sum_i \frac{1}{n_i(r)} \sum_{j=1}^{n_i(r)} (\hat{\mu}_i \cdot \hat{r}_{ij})(\hat{\mu}_j \cdot \hat{r}_{ij}) \right\rangle, \tag{2}$$

$$T(r) = \tfrac{1}{2}[F(r) - L(r)], \tag{3}$$

where $\hat{\mu}_i$ is the dipole unit vector on molecule i, $\hat{r}_{ij}$ is the unit vector in the direction from molecule i to j, and $n_i(r)$ is the number of molecules with center-of-mass distance between r and $r + \delta r$ from molecule i. Results for an infinite homogeneous system were obtained from the MD simulation results by applying the corrections $\delta F = 3\delta L = 3\delta T = -(\varepsilon - 1)^2/(9y\varepsilon N)$,[18,19] where ρ is the molecular number density, μ is the molecular dipole moment, ε is the dielectric constant, and

$$y = \rho\mu^2/(9\varepsilon_0 k_B T) \tag{4}$$

is the dimensionless dipole strength. The correction is $\delta L = -5.9 \times 10^{-6}$ for the simulations with $N = 60\,000$ molecules. The radial pair distribution function $g(r)$ plotted in Fig. 1(a) shows that other molecules are excluded for $r < 0.20$ nm and that positional correlations vanish for $r > 2$ nm. The orientation correlation functions plotted in Figs. 1(b) and 1(c) have been multiplied by the factor r^3 to distinguish the short-range functions, which decrease more rapidly than r^{-3}, from the long-range functions. The orientation correlation function $F(r)$ is short range and $r^3F(r)$ vanishes for r > 2 nm, whereas $r^3L(r)$ and $r^3T(r)$ reach constant long-range limiting values for $r > 2$ nm.

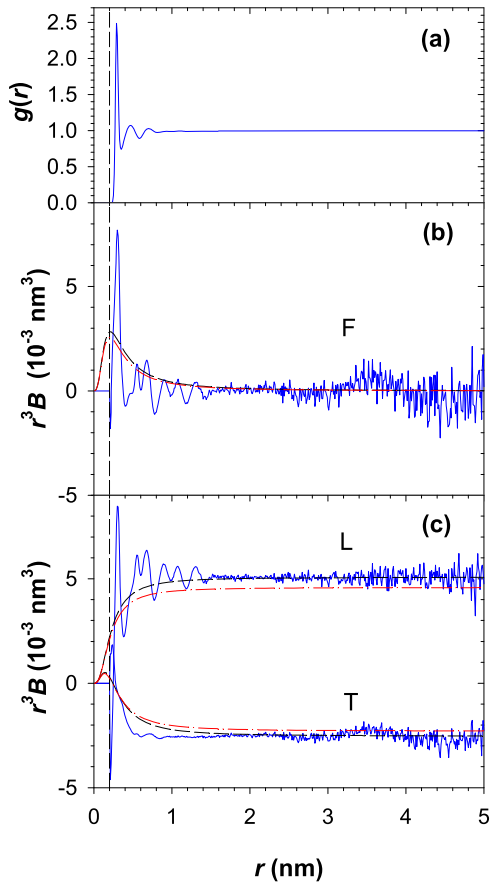

FIG. 1. The solid (blue) curves are the results from TIP4P/2005 water MD simulation for (a) the pair distribution function $g(r)$ and (b) and (c) the orientation correlation functions $F(r)$, $L(r)$, and $T(r)$. The dashed (black) curves in (b) and (c) are the correlation functions given by Eqs. (22) and (23) with the value $a^3 = 5.07 \times 10^{-3}$ nm^3 determined from the MD simulation, while the dashed-dotted (red) curves are the correlation functions with $a^3 = 4.58 \times 10^{-3}$ nm^3 obtained by fitting the HRS data. Orientation correlation functions multiplied by r^3 are plotted to emphasize the long-range part of the functions. The vertical dashed line at 0.20 nm marks the radius of the excluded volume around each molecule.

This work uses the same TIP4P/2005 water MD model as Ref. 11 so that the present results can be directly compared with results from that work. Dipole correlations have also been investigated for SPC/E, SPC/Fd, and swm4-DP potential models in Ref. 17, with simulations of up to 27 648 molecules. The constant offset in $F(r)$ that is corrected by δF can be seen in the inset to Fig. 1 of Ref. 17, and $L(r)$ from Ref. 17 plotted as $r^3L(r)$ in Fig. 2 of Ref. 10 shows the effect of the missing δL correction. The correlation functions vary in detail with the potential model used for the simulation, as can be seen by comparing Fig. 1 with simulation results in Ref. 17. Both Refs. 11 and 17 find that the simulation results have converged for system size about $N = 4000$ molecules.

The dielectric constant ε may be calculated from the mean square fluctuation of the total dipole M, using the expressions $G_K = (\langle M^2 \rangle - \langle M \rangle^2)/(N\langle|\mu|\rangle^2)$ and $\varepsilon = 1 + 3yG_K$, but the accuracy is limited (±2% for a 25 ns run) by slow fluctuations of $\langle M^2 \rangle$ which do not decrease with increasing system size. Smaller statistical error was obtained using the correlation function expression[18]

$$g_K = 1 + 4\pi\rho \int F(r) g(r) r^2 dr \tag{5}$$

for the Kirkwood correlation factor g_K and solving the Kirkwood relation

$$(\varepsilon - 1)(2\varepsilon + 1)/\varepsilon = 9yg_K \tag{6}$$

for ε. The asymptotic limits for the longitudinal and transverse correlation functions are $L(r \to \infty) = a^3 r^{-3}$ and $T(r \to \infty) = -\frac{1}{2}a^3 r^{-3}$, where the value for the correlation length parameter a can be determined using the theoretical result for the longitudinal dipole correlation function $B_L(r)$ for a non-polarizable polar fluid[5,18]

$$a^3 = \lim_{r\to\infty} r^3 B_L(r) = \frac{(\varepsilon - 1)^2}{18\pi\varepsilon\rho y}, \tag{7}$$

with the result for a^3 shown in Table I.

III. HRS OBSERVATIONS

Figure 2 shows measurements from Ref. 6 of the HRS intensity ratios I_{VV}/I_{HV}, I_{HV}/I_{VH}, and I_{HH}/I_{VH} for D_2O as a function of scattering angle θ_s. Scattering configurations with incident and scattered light polarized either perpendicular or parallel to the horizontal scattering plane are denoted as VV, HV, VH, and HH, where V denotes vertical polarization, H denotes horizontal polarization, and the first and second letters refer to the incident and scattered light, respectively. The expressions fit to the HRS intensity ratio data are[5,6,10]

$$I_{VV} = A_0 P^2 + A_T R^2, \tag{8}$$

$$I_{HV} = A_0 + A_T, \tag{9}$$

$$I_{VH} = A_0 + A_T \sin^2(\theta_s/2) + A_L \cos^2(\theta_s/2), \tag{10}$$

$$\begin{aligned} I_{HH} = {} & A_0[\sin^2\theta_s + P^2\cos^2\theta_s] \\ & + A_T[1 - (R-1)\cos\theta_s]^2 \sin^2(\theta_s/2) \\ & + A_L[1 + (R-1)\cos\theta_s]^2 \cos^2(\theta_s/2), \end{aligned} \tag{11}$$

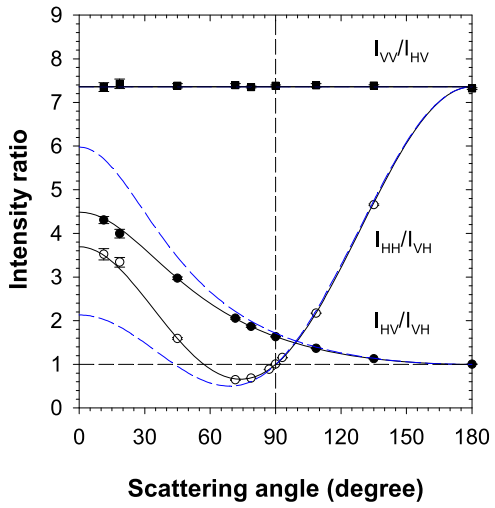

FIG. 2. HRS intensity ratios measured for water from Ref. 6. The solid curves are the fit to the data (symbols) using Eqs. (8)–(11) with the parameters P^2 = 1.50, R = 2.900 ± 0.005, A_T/A_0 = 5.571 ± 0.128, and A_L/A_T = 0.0834 ± 0.0044. Incoherent HRS gives curves symmetric around θ_s = 90° (vertical dashed line) and I_{HV}/I_{VH} = 1 (horizontal dashed line). The dashed (blue) curves are the results obtained using $a^3 = 5.07 \times 10^{-3}$ nm^3 from the MD simulation, whereas the solid curves are obtained using $a^3 = 4.58 \times 10^{-3}$ nm^3 instead.

TABLE II. HRS results calculated from a 25 ns MD trajectory using Eqs. (13) and (14) with $K = 0$ are shown, for three β tensors specified by A and B. Fully incoherent HRS results (inc subscript) are also given for comparison. The number in parentheses is the statistical uncertainty of the last digits, estimated from the fluctuations for five successive 5 ns segment of the trajectory. The last column gives experimental HRS values taken from the solid fitted curves in Fig. 2.

	θ_s (deg)	Vector β	Octupolar β	Mixed β[a]	Expt.[b]
A		1/3	−1/2	0.68	
B		1/3	−1/2	−0.20	
$(I_{VV}/I_{HV})_{inc}$	0	9	3/2	4.434	
	90	9	3/2	4.434	
	180	9	3/2	4.434	
$(I_{HV}/I_{VH})_{inc}$	0	1	1	1	
	90	1	1	1	
	180	1	1	1	
$(I_{HH}/I_{VH})_{inc}$	0	9	3/2	4.434	
	90	1	1	1	
	180	9	3/2	4.434	
$(I_{VV})_{inc}$	0	1/3	1/7	0.3310	
	90	1/3	1/7	0.3310	
	180	1/3	1/7	0.3310	
$I_{VV}/(I_{VV})_{inc}$	0	3.20 (14)	1.11 (5)	2.69 (12)	
	90	3.20 (14)	1.11 (5)	2.69 (12)	
	180	3.20 (14)	1.11 (5)	2.69 (12)	
I_{VV}/I_{HV}	0	9.0000 (0)	1.52 (6)	7.34 (13)	7.36
	90	9.0000 (0)	1.52 (6)	7.34 (13)	7.36
	180	9.0000 (0)	1.52 (6)	7.34 (13)	7.36
I_{HV}/I_{VH}	0	0.96 (5)	1.11 (7)	0.98 (4)	4.49
	90	1.03 (6)	1.08 (5)	1.00 (5)	1.64
	180	0.96 (5)	1.11 (7)	0.98 (4)	1.00
I_{HH}/I_{VH}	0	9.0000 (0)	1.62 (4)	7.46 (11)	3.69
	90	1.0000 (0)	1.06 (2)	0.97 (3)	1.00
	180	9.0000 (0)	1.62 (4)	7.46 (11)	7.36

[a]Reference 11.
[b]Reference 6.

with the fit parameters P^2 = 1.500, R = 2.900 ± 0.005, A_T/A_0 = 5.571 ± 0.128, and A_L/A_0 = 0.465 ± 0.022 [A_L/A_T = 0.0834 ± 0.0044]. The fitted curves obtained using Eqs. (8)–(11) are invariant for changes to alternative parameters P'^2, A'_T/A'_0, A'_L/A'_0, where

$$\frac{R^2 - P'^2}{R^2 - P^2} = \frac{1 + A'_T/A'_0}{1 + A_T/A_0} = \frac{1 + A'_L/A'_0}{1 + A_L/A_0}. \tag{12}$$

Data for $\theta_s < 10°$ are not shown since it follows a more complicated function due to the divergence of the focused laser beam. The values from the fitted curves for the HRS intensity ratios at θ_s = 0°, 90°, and 180° are given in the last column of Table II. The fitted curves are not symmetric around θ_s = 90°, and $I_{HV}/I_{VH} \neq 1$, two observations that incoherent HRS cannot account for.

IV. SHORT RANGE HRS

HRS including the effect of molecular correlation at distances less than the box length can be calculated directly from the MD simulation trajectory and the molecular hyperpolarizability tensor. The Cartesian tensor expression for the

second-harmonic dipole induced in a molecule by the optical electric field at frequency ω is

$$\begin{aligned}\mu_i(2\omega) &= \beta_{ijk}(-2\omega;\omega,\omega)E_j(\omega)E_k(\omega)\\ &= a_{i\alpha}a_{j\beta}a_{k\gamma}\beta_{\alpha\beta\gamma}(-2\omega;\omega,\omega)E_j(\omega)E_k(\omega),\end{aligned} \quad (13)$$

where β_{ijk} and $\beta_{\alpha\beta\gamma}$ are the lab frame and molecule frame hyperpolarizability tensors, respectively, and $a_{i\alpha}$ is the direction cosine between the lab i axis and the molecule α axis. The scattered field radiated by the induced molecular dipoles oscillating at the second-harmonic frequency, summed over molecules b at positions $\vec{r}_b$, is

$$E_i(2\omega) \propto \sum_b \beta_{ijk,b}\exp(i\vec{K}\cdot\vec{r}_b)E_jE_k, \quad (14)$$

where the scattering vector is $\vec{K} = 2\vec{k}(\omega) - \vec{k}(2\omega)$ and the HRS intensity is $I_i(2\omega) \propto |E_i(2\omega)|^2$.

HRS intensities calculated including correlations will be compared to HRS from uncorrelated, randomly oriented molecules, where the individual molecule contributions add incoherently and the HRS intensity is proportional to the isotropic average $\left\langle \beta_{ijk}^2 \right\rangle$. Expressions have been derived for these isotropic averages in terms of the β Cartesian tensor components and also in terms of β spherical tensor components.[3,4,10,20] For the water molecule with C_{2v} symmetry, the 7 non-vanishing molecule-frame components are β_{zzz}, β_{zxx}, $\beta_{xxz} = \beta_{xzx}$, β_{zyy}, and $\beta_{yyz} = \beta_{yzy}$, where z is the 2-fold axis, y is perpendicular to the molecular plane, and permutation symmetry for the last indices follows from the indistinguishability of the two applied fields. The tensor can be specified by β_{zzz} and the four ratios $A = \beta_{zxx}/\beta_{zzz}$, $A' = \beta_{xxz}/\beta_{zzz}$, $B = \beta_{zyy}/\beta_{zzz}$, and $B' = \beta_{yyz}/\beta_{zzz}$. Far from resonance, there is approximate permutation symmetry for all indices (Kleinman symmetry), which gives $A = A'$ and $B = B'$ and reduces to 3 the number of independent tensor components. For incoherent HRS with C_{2v} and Kleinman symmetry, one has[4,20]

$$\begin{aligned}(I_{VV})_{inc} &\propto \left\langle \beta_{ZZZ}^2 \right\rangle / \beta_{zzz}^2\\ &= (1/35)\left[5 + 6(A+B) + 9(A^2+B^2) + 6AB\right], \quad (15)\\ (I_{HV})_{inc} &\propto \left\langle \beta_{ZXX}^2 \right\rangle / \beta_{zzz}^2\\ &= (1/105)\left[3 - 2(A+B) + 11(A^2+B^2) - 2AB\right], \quad (16)\end{aligned}$$

and β is the direct sum of irreducible spherical tensors of first and third rank (vector β and octupolar β).[4,10] The limiting case of pure vector β, with HRS intensity ratio $(I_{VV}/I_{HV})_{inc} = 9$, is obtained for $A = B = 1/3$, while the opposite limiting case of pure octupolar β, with $(I_{VV}/I_{HV})_{inc} = 3/2$, is obtained for $A + B = -1$. Table II gives the incoherent HRS results calculated for three combinations of A and B, producing vector, octupolar, and mixed β tensors.

The effect of molecular correlations is addressed by evaluating Eqs. (13) and (14) directly from the MD trajectory for TIP4P/2005 water. The fluctuating total induced second-harmonic dipole and HRS intensity are obtained by summing over all the molecules in the box for each frame of the trajectory. The scattering wave vector magnitude for the HRS measurements in Fig. 2 ranges from 0.0030 nm^{-1} at 11° to 0.031 nm^{-1} at 180°, but wave vectors satisfying the MD periodic boundary condition for a box of length L have components $k_m = 2\pi m/L$, where the smallest non-zero wave number $k_1 = 0.516\ nm^{-1}$ is much larger than the largest scattering wave number K in the HRS experiment. HRS results calculated from the MD trajectory using $K = k_0 = 0$ in Eq. (14) are given in Table II. The statistical uncertainty of the results was estimated from the fluctuations for the five successive 5 ns segments of the trajectory.

The results given in Table II for vector β are the same for HRS with correlations and for incoherent HRS, except for a 3.20 × increase in I_{VV}. This factor is just equal to G_K, the increase in the mean square total dipole moment due to correlations in the MD simulation. These factors are equal since the dipole vector and vector β are sensitive to the same correlations. The Kirkwood factor g_K measures the effect of dipole vector correlations for an infinite homogeneous medium, and G_K overestimates g_K by about 50% in this simulation (see Table I). The HRS results for octupolar β are increased by 5%–10% compared to the results for fully incoherent HRS. This increase is comparable to or larger than the 5% uncertainty due to fluctuations, is larger than expected, and may in part be an artefact due to the cubic simulation box. The third β tensor example uses the best fit values for A and B from Ref. 11 and has mixed vector and octupolar β contributions. The vector part is dominant, so the increase in I_{VV}/I_{HV} compared to incoherent HRS is close to that for the vector β example. Otherwise, the angle and polarization dependence have the same form as for incoherent HRS. In particular, the HRS results calculated from the MD simulation are symmetric about $\theta_s = 90°$, and $I_{HV}/I_{VH} = 1$. HRS calculated directly from the MD simulation does not have the key features seen in the experimental HRS results, given for comparison in the last column of Table II.

The above result is contrary to the results presented in Ref. 11. The most direct comparison is between the mixed β results in Table II of this work and the results shown in Fig. 1(c) of Ref. 11 since both are calculated using exactly the same β tensor and MD model. And despite the difference in notation, the calculation using Eq. (14) in this work is identical to the calculation using Eq. (1) or its reformulation as Eq. (4) in Ref. 11. However, the calculated values for I_{HV}/I_{VH} at $\theta_s = 0°$, 90°, and 180° are 1.0, 1.0, and 1.0 from Table II (mixed β column) in this work, as compared to 4.0, 1.8, and 1.0 from Fig. 1(c) in Ref. 11. The conclusion in Ref. 11 that short-range correlations fully account for the HRS observations is based on these results, which are incompatible with the results for I_{HV}/I_{VH} from the present work.

The results in this work and Ref. 11 are given at $K = 0$, and the only apparent difference in the calculations is how the $K = 0$ results are obtained. The results in Table II are calculated at $K = 0$, whereas the results in Ref. 11 are obtained by extrapolating results calculated for K in the range $0.3 < K < 10\ nm^{-1}$ to $K = 0$, as shown in Fig. S4 of Ref. 11. To understand the effect of this calculation difference, Fig. 3 shows $I_{VV}/(I_{VV})_{inc}$ and I_{HV}/I_{VH} for vector β ($A = B = 1/3$) and $\theta_s = 90°$, computed from the MD simulation for a range of K values. The computed results at $K = 0$ differ insignificantly from the predicted values $I_{VV}/(I_{VV})_{inc} = G_K$ and $I_{HV}/I_{VH} = 1$. The HRS results computed at the experimental K value also are insignificantly

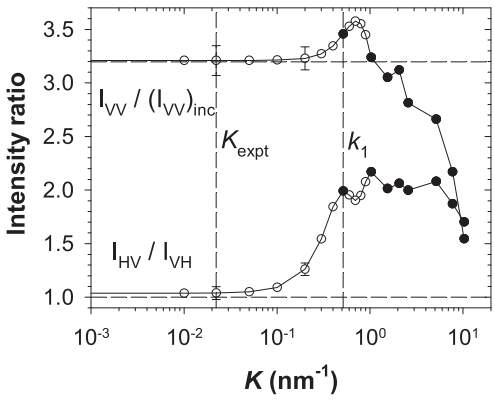

FIG. 3. HRS results calculated for a 5 ns MD simulation trajectory using Eqs. (13) and (14), for pure vector β and 90° scattering angle, are shown as a function of K [for the scattering wave vector (0, K, 0)] by open circles joined by solid lines. The representative error bars shown for several points are the standard deviation for results calculated from successive 5 ns segments of the simulation. The HRS experimental results were obtained at $K = 0.022$ nm^{-1}, marked by the left vertical dashed line. The right vertical dashed line marks $K = k_1$, and points satisfying PBC (filled circles) are plotted at $K = mk_1$ for $m = 1$, 2, 3, 4, 5, 10, 15, and 20. The horizontal dashed lines mark the $K = 0$ expected values $I_{VV}/(I_{VV})_{inc} = G_K = 3.196$ and $I_{HV}/I_{VH} = 1$. The values $I_{VV}/(I_{VV})_{inc} = 3.21 \pm 0.14$ and $I_{HV}/I_{VH} = 1.04 \pm 0.05$ at $K = 0$ are calculated for this 5 ns simulation trajectory. A fourth-degree polynomial fit to the filled circles and extrapolated to $K = 0$, as in Ref. 11, gives $I_{VV}/(I_{VV})_{inc} = 3.73$ and $I_{HV}/I_{VH} = 2.08$.

different from the $K = 0$ values. However, the results for $K = 0$ and for $K \geq k_1$ are very different. The extrapolation in Ref. 11 uses only results for K values satisfying PBC, $K = k_m = 2\pi m/L$, but excludes the results for $m = 0$, which is the first and most important K value for this calculation. Extrapolating the results at $K = k_m$ for $m \geq 1$ (the filled circles in Fig. 3), using a fourth-degree polynomial as stated for Fig. S4 of Ref. 11, gives $I_{VV}/(I_{VV})_{inc} = 3.73$ and $I_{HV}/I_{VH} = 2.08$. These results, obtained by extrapolation of just the high K points, are very poor approximations to the values at $K = 0$, and this appears to be the source of the disagreement between the present results and the results in Ref. 11. The results directly evaluated at $K = 0$ are the correct results for this calculation.

The MD simulation approximates a liquid of infinite extent using a finite cell with periodic boundary conditions. The periodicity of the system is strictly enforced during the simulation, so every frame of the MD simulation with PBC specifies an infinite perfect single crystal with lattice spacing equal to the box length. Liquid properties are calculated by treating the simulation cell instead as if it is a small sample from an infinite non-periodic system. The HRS sum in Eq. (14) evaluated for a single simulation cell is a Fourier transform with continuous spectrum, the sum is well behaved at $K = 0$, and it is simple and direct to calculate the HRS intensities at $K = 0$ or at small K. Correlations with short range compared to the simulation box length are correctly treated by the sum over the simulation box but do not account for the HRS observations. Correlations with long range compared to the simulation box are not adequately treated by this sum over the simulation box. Since the volume integral of r^{-3} diverges logarithmically, the effect of dipole correlations that vary as r^{-3} requires a more careful treatment of the $K = 0$ limit, which is given in Sec. V.

V. LONG RANGE HRS

The long-range coherent contribution to HRS is due to dipole correlations and vector β. The molecular dipoles in liquid water form a random vector field, and the most general pair correlation function for a homogeneous, isotropic random vector field $\vec{U}(\vec{r})$ has the form[10,21]

$$B_{\alpha\beta}(\vec{r}) = \langle U_\alpha(\vec{0}) U_\beta(\vec{r})\rangle = B_T(r)[\delta_{\alpha\beta} - r_\alpha r_\beta/r^2] + B_L(r) r_\alpha r_\beta/r^2, \quad (17)$$

where $B_T(0) = B_L(0)$. The tensor $B_{\alpha\beta}$ is diagonal when one coordinate axis is aligned along $\vec{r}$, with the transverse and longitudinal correlation functions B_T and B_L as the diagonal components. The corresponding spatial spectrum is

$$S_{\alpha\beta}(\vec{K}) = \int d^3 r B_{\alpha\beta}(\vec{r}) \exp(i\vec{K}\cdot\vec{r}) = S_T(K)[\delta_{\alpha\beta} - K_\alpha K_\beta/K^2] + S_L(K) K_\alpha K_\beta/K^2, \quad (18)$$

where the tensor $S_{\alpha\beta}$ is diagonal when one coordinate axis is aligned along the scattering vector $\vec{K}$, with the transverse and longitudinal spectra S_T and S_L as the diagonal components.

HRS intensities with the functional form given by Eqs. (8)–(11) are obtained by expressing HRS from the vector part of β in terms of the vector correlation functions in Eq. (17).[10] The intensity coefficients A_T and A_L are proportional to $S_T(K)$ and $S_L(K)$. The expressions for S_T and S_L obtained by substituting Eq. (17) for $B_{ij}(\vec{r})$ into the integral in Eq. (18), transforming to polar coordinates, and integrating are[10]

$$S_T(K) = 4\pi \int_0^\infty r^2 dr \left[\left\{ j_0(Kr) - \frac{j_1(Kr)}{Kr} \right\} B_T(r) + \frac{j_1(Kr)}{Kr} B_L(r) \right], \quad (19)$$

$$S_L(K) = 4\pi \int_0^\infty r^2 dr \left[2\frac{j_1(Kr)}{Kr} B_T(r) + \left\{ j_0(Kr) - 2\frac{j_1(Kr)}{Kr} \right\} B_L(r) \right], \quad (20)$$

where $j_n(x)$ are spherical Bessel functions.

An arbitrary isotropic random vector field can be represented as the sum of two uncorrelated isotropic vector fields, one of which is solenoidal (zero divergence) and one of which is potential (zero curl).[21] For an uncharged, homogeneous dielectric with zero applied electric field, $\vec{\nabla}\cdot\vec{D} = \vec{\nabla}\cdot\varepsilon\vec{E} = \vec{\nabla}\cdot(\varepsilon_0\vec{E} + \vec{P}) = 0$ and $\vec{\nabla}\cdot\vec{P} = 0$ for the polarization $\vec{P}$, so the dipole vector field is solenoidal in the unperturbed liquid. The condition on the correlation function for a solenoidal field, for which $S_L(K) = 0$, is[21]

$$B_T(r) = B_L(r) + \frac{r}{2}\frac{d}{dr} B_L(r). \quad (21)$$

A correlation function for a solenoidal vector field which has the r^{-3} asymptotic dependence for dipole-dipole correlation in a polar liquid is[10]

$$B_L(r) = [1 + (r/a)^2]^{-3/2}, \quad (22)$$

$$B_T(r) = [1 + (r/a)^2]^{-3/2}[1 - \tfrac{3}{2} r^2/(r^2 + a^2)]. \quad (23)$$

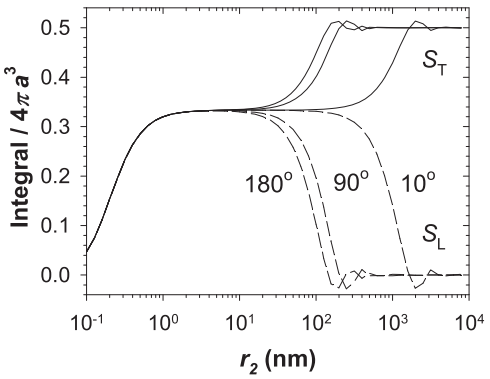

FIG. 4. Integrals for S_T (solid curves) and S_L (dashed curves) given by Eqs. (19) and (20), for the correlation functions given by Eqs. (22) and (23), are plotted as a function of the upper integration limit r_2, for $\theta_s = 10°$, 90°, and 180° ($K = 0.0027$, 0.022, and 0.031 nm^{-1}). Both short-range and long-range correlations increase the HRS intensity, but the difference between S_T and S_L is due entirely to correlations at distances $r_2 > 10$ nm. The final value for the S_T and S_L integrals is approached when correlations at distances up to $r_2 > 500$ nm are included, where r_2 diverges as $\theta_s \to 0$.

This correlation function, with $a^3 = 5.07 \times 10^{-3}$ nm^3 determined from the MD simulation, is plotted as the dashed curves in Figs. 1(b) and 1(c). This function accurately represents the MD correlation functions $F(r)$, $L(r)$, and $T(r)$ for $r > 2$ nm and is a rough approximation for $r < 2$ nm.

Evaluating the integrals in Eqs. (19) and (20) using the correlation functions given by Eqs. (22) and (23) gives the spectra[10]

$$S_T(K) = 2\pi a^3 K a K_1(Ka), \tag{24}$$

$$S_L(K) = 0, \tag{25}$$

where $K_n(x)$ is the modified Bessel function of the second kind, of order n. The value of $S_T(K)$ for small K is nearly constant, with the $K = 0$ value[10]

$$S_T(0) = 2\pi a^3. \tag{26}$$

The range of the correlations that make the main contribution to the coherent HRS spectrum depends on K. Figure 4 shows results for the integrals in Eqs. (19) and (20), for the correlation function given by Eqs. (22) and (23), but with upper integration limit r_2. For $a << r_2 << K^{-1}$, the integrals give $S_T(r_2) = S_L(r_2) = 4\pi a^3/3$, whereas for $a << r_2$ and $K^{-1} << r_2$, the integrals give $S_T(r_2) = 4\pi a^3/2$ and $S_L(r_2) = 0$. For the values of a and K in the HRS experiment for water, the first result is obtained for $r_2 \approx 3$ nm, while the second result is obtained for $r_2 \approx 300$ nm at $\theta_s = 180°$ and 3000 nm at $\theta_s = 10°$. When only correlations at distances up to $r_2 \approx 3$ nm are included, the HRS intensity is increased but the form remains the same as for incoherent HRS. The observed HRS with $S_T \neq S_L$ ($A_T \neq A_L$) is obtained when correlations at distances up to $r_2 \approx 300$–3000 nm are included.

VI. HYPERPOLARIZABILITY AND DIPOLE CORRELATION OF WATER

The molecular hyperpolarizability and orientation correlation combine to determine the HRS intensities, and conversely, one may use HRS observations to solve for the molecular hyperpolarizability and orientation correlation. To allow for a different treatment of the vector and octupolar β HRS contributions, the tensor β is expressed as the direct sum of four irreducible spherical tensors,[4]

$$\beta = \beta^{[ss,1]} \oplus \beta^{[ms,1]} \oplus \beta^{[ms,2]} \oplus \beta^{[ss,3]}, \tag{27}$$

where $\beta_m^{[\nu,l]}$ is a spherical tensor of rank l with $2l + 1$ components m, index ν labels the symmetry under permutation of the Cartesian tensor indices (ss is totally symmetric, while ms is non-symmetric for the first index permutations), and the mixed symmetry ν = ms tensors vanish when Kleinman symmetry holds. For C_{2v} symmetry, the seven non-vanishing spherical components are[4]

$$\beta_0^{[ss,1]}/\beta_{zzz} = (-i/\sqrt{15})\,[3 + (A + 2A') + (B + 2B')]\,, \tag{28}$$

$$\beta_0^{[ms,1]}/\beta_{zzz} = (-i/\sqrt{3})\,[(A - A') + (B - B')]\,, \tag{29}$$

$$\beta_{\pm2}^{[ms,2]}/\beta_{zzz} = (\mp i/\sqrt{6})\,[(A - A') - (B - B')]\,, \tag{30}$$

$$\beta_0^{[ss,3]}/\beta_{zzz} = (-i/\sqrt{10})\,[-2 + (A + 2A') + (B + 2B')]\,, \tag{31}$$

$$\beta_{\pm2}^{[ss,3]}/\beta_{zzz} = (+i/\sqrt{12})\,[(A + 2A') - (B + 2B')]\,. \tag{32}$$

(The entry in Table II of Ref. 4 for ν = ss, $l = 3$, $m = 0$, ijk = zzz should have a + sign.)

HRS intensities I_{VV} and I_{HV} expressed in terms spherical tensor components are[4,10]

$$I_{VV} = R^2 A_T + P^2 A_0 = C_T \frac{9}{45}\left|\beta_0^{[ss,1]}\right|^2 + \frac{6}{105}\left|\beta^{[ss,3]}\right|^2, \tag{33}$$

$$I_{HV} = A_T + A_0 = C_T \frac{1}{45}\left|\beta_0^{[ss,1]} + \sqrt{5}\beta_0^{[ms,1]}\right|^2 + \frac{1}{15}\left|\beta^{[ms,2]}\right|^2 + \frac{4}{105}\left|\beta^{[ss,3]}\right|^2, \tag{34}$$

where $|\beta^{[\nu,l]}|^2 = \sum_m |\beta_m^{[\nu,l]}|^2$. The β components with $l = 1$ transform as vectors under rotations, and $R^2 = (I_{VV}/I_{HV})_{l=1}$ is the HRS intensity ratio due to just these terms. Similarly, $P^2 = (I_{VV}/I_{HV})_{l=2,3}$ is the HRS intensity ratio due to just the terms with $l = 2$ and 3. Dipole orientation correlation affects only the $l = 1$ HRS contribution, increasing the $l = 1$ terms in I_{VV} and I_{HV} by the factor C_T. Possible quadrupolar and octupolar orientation correlation effects for the $l = 2$ and 3 terms are ignored. The β tensor components determine R^2 and P^2, dipole correlations determine C_T, and both combined determine A_T/A_0 and I_{VV}/I_{HV}. With C_T determined from the MD simulation, one can solve for β tensor component ratios A, A', B, and B' that fit the observed values for I_{VV}/I_{HV}, R^2, and A_T/A_0, where the dependence of A_T/A_0 on $P^2(A, A', B, B')$ is given by Eq. (12).

The HRS intensity factor C_T accounting for vector β correlation effects is calculated from the MD orientation correlation functions using Eqs. (19) and (20), with the integrals evaluated piecewise over three regions,[5,10]

$$S_T = S_{T,1} + S_{T,2} + S_{T,3}, \tag{35}$$

$$S_L = S_{L,1} + S_{L,2} + S_{L,3}. \tag{36}$$

The delta function self-correlation in region 1 ($r < r_1 = 0.20$ nm) gives

$$S_{T,1} = S_{L,1} = (1/3)(4\pi r_0^3/3), \tag{37}$$

where $4\pi r_0^3/3 = \rho^{-1}$ is the volume per molecule, $r_0 = 0.1928$ nm, and $S_{T,1} = S_{L,1} = 10.010 \times 10^{-3}$ nm^3 for TIP4P/2005 water. In region 2 ($r_1 < r < r_2 = 5.0$ nm), the correlation functions $B_L(r) = L(r)$ and $B_T(r) = T(r)$ obtained from the MD simulation are integrated to give $S_{T,2}$ and $S_{L,2}$. At short range, where $Kr << 1$, it is a good approximation to take the $K = 0$ limit for the integrand in Eqs. (19) and (20), which gives

$$S_{T,2} = S_{L,2} = 4\pi \int_{r_1}^{r_2} r^2 dr g(r)[B_L(r) + 2B_T(r)]. \tag{38}$$

The contribution from region 3 ($r > r_2 = 5.0$ nm) is obtained by subtracting $S_{TL,3}$ from Eqs. (25) and (26),

$$S_{T,3} = 2\pi a^3 - S_{TL,3}, \tag{39}$$

$$S_{L,3} = 0 - S_{TL,3}, \tag{40}$$

where

$$\begin{aligned} S_{TL,3} &= 4\pi \int_0^{r_2} r^2 dr[B_L(r) + 2B_T(r)] \\ &= 4\pi \int_0^{r_2} r^2 dr[1 + (r/a)^2]^{-5/2} \\ &= (4\pi a^3/3)[1 + (a/r_2)^2]^{-3/2} \end{aligned} \tag{41}$$

is obtained using the $K = 0$ limit for the integrand in Eqs. (19) and (20), with Eqs. (22) and (23) for the correlation functions. For the values $K < 0.03$ nm^{-1} probed by the experiment, Eq. (41) differs from the exact integral by <0.3%. [The $K = 0$ limit is incorrectly evaluated in Eqs. (22) and (23) of Ref. 10 and Eqs. (35), (36), (38), and (39) of Ref. 5.]

Table III shows the vector β HRS intensity contributions calculated using Eqs. (35)–(41) with the correlation length parameter $a^3 = 5.07 \times 10^{-3}$ nm^3 [obtained from the MD simulation using Eq. (7)]. The three contributions to the transverse spectrum are about equal, but for the longitudinal spectrum, the long-range correlation contribution nearly cancels the self-correlation and short-range contributions. The result is a nearly pure transverse spectrum with $S_L/S_T = 0.018$ and with the HRS intensity S_T larger by the factor $C_T = S_T/S_{T,1} = 3.242$ than the intensity $S_{T,1}$ that would be obtained for vector β HRS in the absence of orientation correlation. There are multiple combinations of the β component ratios A, A', B, and B' which fit the observed values of I_{VV}/I_{HV}, R^2, and A_T/A_0 for this value of a^3. However, using this a^3 gives S_L/S_T much smaller than A_L/A_T from the fit to the HRS data and results in a very poor fit to the data, as shown by the dashed curves in Fig. 2.

TABLE III. The values at $K = 0$ for the transverse (T) and longitudinal (L) components of the vector HRS spatial spectra are obtained by integrating the orientation correlation functions for water [see Eqs. (35)–(41)]. The total integrals and the piecewise contributions from the self-correlation (1), short-range (2) and long-range (3) regions are given for two values of the long-range orientation correlation strength a^3.

Property	MD	HRS fit
a^3 (10^{-3} nm^3)	5.072	4.584
$S_{T,1} = S_{L,1}$ (10^{-3} nm^3)	10.010	10.010
$S_{T,2} = S_{L,2}$ (10^{-3} nm^3)	11.783	11.783
$S_{T,3}$ (10^{-3} nm^3)	10.661	9.634
$S_{L,3}$ (10^{-3} nm^3)	−21.209	−19.172
S_T (10^{-3} nm^3)	32.454	31.426
S_L (10^{-3} nm^3)	0.583	2.621
S_L/S_T	0.0180	0.0834
$C_T = S_T/S_{T,1}$	3.242	3.140

The correlation strength parameter a^3 may be overestimated by the MD simulation since non-polarizable models such as TIP4P/2005 tend to overestimate the molecular dipole to compensate for the lack of polarizability. An even larger value $a^3 = 6.07 \times 10^{-3}$ nm^3 is obtained from a MD simulation with the simple point charge (SPC) water model.[14] One may treat a^3 as an adjustable parameter, to be determined from the fit to the observed values for I_{VV}/I_{HV}, R^2, A_T/A_0, and A_L/A_0. An essentially exact fit is obtained for a continuum of combinations of the β component ratios, with A, A', B, and B' in the range from −0.1 to +1.3, a^3 in the range from 4.40 to 4.59 $\times 10^{-3}$ nm^3, and C_T in the range from 3.10 to 3.14. Most of the solutions exhibit large deviations from Kleinman symmetry, with P^2 as low as 0.1. However, the solutions with small deviations from Kleinman symmetry are clustered near the solution $(A, A', B, B', a^3) = (0.150, 0.149, 0.880, 0.840, 4.584 \times 10^{-3}$ nm$^3)$ with $P^2 = 1.498$ and $C_T = 3.140$. The last column of Table III shows the calculation giving $S_L/S_T = A_L/A_T = 0.0834$ using this value of a^3. The value obtained for a^3 from the fit depends on the model-dependent short-range correlation contribution $S_{T,2}$ calculated from the MD simulation. A 10% change in $S_{T,2}$ produces a 5% change in a^3 (and C_T), and the largest uncertainty for a^3 may be due to the systematic uncertainty for $S_{T,2}$. Nevertheless, a^3 obtained by fitting the HRS experimental value for A_L/A_T provides the most direct available experimental determination for the long-range correlation strength. This HRS result for a^3 is 10% smaller than the TIP4P/2005 MD result.

The β tensor component ratios $(A, A', B, B') = (0.150, 0.149, 0.880, 0.840)$ from the example HRS fit are similar to the result $A = A' = 0.138$ and $B = B' = 1.02$ for the liquid phase model II in Ref. 22. This is an *ab initio* calculation at the Moller-Plesset MP2 level of theory, for the static hyperpolarizability of the water molecule in a local environment with a strong axial field and symmetric field gradient. The effect of the local environment is to induce an increment $\Delta\beta$ large enough to reverse the sign of β (with respect to the dipole). A Hartree-Fock semicontinuum model calculation gives $(A, A', B, B') = (0.256, 0.287, 1.376, 1.363)$ at the laser frequency for the HRS measurements.[23] The deviations from Kleinman symmetry are −12% (A/A') and +1% (B/B') for this model, as compared to 1% and 5% for the HRS fit example. The effects of intermolecular interactions and orientation correlations for liquid phase HRS can be separated by fitting the HRS data and then setting the correlation factor $C_T = 1$ in Eqs. (33) and (34). The resulting value I_{VV}/I_{HV} is in the range 5.84–6.01 for all the fits and is 5.92 for the particular A, A', B, B' example given above. This value of I_{VV}/I_{HV} for a molecule in the liquid is smaller than the value 8.02 ± 0.05 measured in the gas phase,[20]

so the magnitude of vector β is decreased relative to octupolar β for a molecule in the liquid.

VII. SUMMARY AND CONCLUSION

The trajectory obtained from a MD simulation has been used to calculate the molecular orientation correlation functions and also to directly compute HRS including molecular correlation. Molecular position and orientation correlation result from the combined effects of the interactions represented in the MD model, and dipole interactions make a major contribution to orientation correlation. Due to the long range of this interaction, the calculated results are sensitive to the MD simulation boundary conditions, and the short-range coherent contribution to the HRS intensity is overestimated. The long-range contribution is completely missed in the direct calculation of HRS from the MD simulation trajectory due to the small size of the simulation cell.

HRS for water is dominated by the vector part of β, so the HRS intensities can be calculated using the dipole correlation function determined from the MD simulation trajectory, after applying the known boundary condition corrections for a fluid of rigid dipoles. The dipole correlation function has transverse and longitudinal components, and the HRS spectrum due to the vector part of β sees these dipole correlations and has transverse and longitudinal contributions. The dipole correlations at short range give equal transverse and longitudinal spectral contributions, but when long-range correlations are included, the longitudinal spectrum nearly vanishes. This is the origin of the distinctive polarization and angle dependence observed for HRS from water and other polar liquids. The asymmetry between the transverse and longitudinal HRS spectral components depends on the strength of the long-range orientation correlation, so the fit to the observed asymmetry provides an experimental determination of the long-range orientation correlation strength.

ACKNOWLEDGMENTS

This work was supported by the National Science Foundation (NSF) through Grant No. CHE-1212114.

[1] J. Campo, F. Desmet, W. Wenseleers, and E. Goovaerts, Opt. Express **17**, 4587 (2009).
[2] K. Clays and A. Persoons, Phys. Rev. Lett. **66**, 2980 (1991).
[3] R. Bersohn, Y. Pao, and H. L. Frisch, J. Chem. Phys. **45**, 3184 (1966).
[4] P. D. Maker, Phys. Rev. A **1**, 923 (1970).
[5] D. P. Shelton, J. Chem. Phys. **144**, 234506 (2016).
[6] D. P. Shelton, J. Chem. Phys. **141**, 224506 (2014).
[7] D. P. Shelton, J. Chem. Phys. **136**, 044503 (2012).
[8] D. P. Shelton, J. Opt. Soc. Am. B **17**, 2032 (2000); Erratum **34**, 1550 (2017).
[9] D. P. Shelton, J. Chem. Phys. **138**, 154502 (2013).
[10] D. P. Shelton, J. Chem. Phys. **143**, 134503 (2015); Erratum **146**, 199901 (2017).
[11] G. Tocci, C. Liang, D. M. Wilkins, S. Roke, and M. Ceriotti, J. Phys. Chem. Lett. **7**, 4311 (2016).
[12] M. J. Abraham, D. van der Spoel, E. Lindahl, B. Hess, and GROMACS Development Team, GROMACS User Manual Version 5.0.6, www.gromacs.org, 2015.
[13] J. L. F. Abascal and C. Vega, J. Chem. Phys. **123**, 234505 (2005).
[14] J. Zielkiewicz, J. Chem. Phys. **123**, 104501 (2005).
[15] M. Shirts, D. L. Mobley, J. D. Chodera, and V. S. Pande, J. Phys. Chem. B **111**, 13052 (2007).
[16] G. Bussi, D. Donadio, and M. Parrinello, J. Chem. Phys. **126**, 014101 (2007).
[17] C. Zhang and G. Galli, J. Chem. Phys. **141**, 084504 (2014).
[18] V. Ballenegger and J.-P. Hansen, Mol. Phys. **102**, 599 (2004).
[19] J. M. Caillol, J. Chem. Phys. **96**, 7039 (1992).
[20] D. P. Shelton, J. Chem. Phys. **137**, 044312 (2012); Erratum **146**, 209903 (2017).
[21] A. S. Monin and A. M. Yaglom, in *Statistical Fluid Mechanics: Mechanics of Turbulence* (MIT Press, Cambridge, MA, 1975), Vol. 2, Chap. 6.
[22] A. V. Gubskaya and P. G. Kusalik, Mol. Phys. **99**, 1107 (2001).
[23] K. O. Sylvester-Hvid, K. V. Mikkelsen, P. Norman, D. Jonsson, and H. Agren, J. Phys. Chem. A **108**, 8961 (2004).